The Cryosphere Discuss., https://doi.org/10.5194/tc-2017-107
Manuscript under review for journal The Cryosphere
Discussion started: 17 July 2017

The Cryosphere Discussions
Open Access
EGU

Near surface meltwater storage in low-density bare ice of the Greenland ice sheet ablation zone

Matthew G. Cooper[1], Laurence C. Smith[1], Asa K. Rennermalm[2], Clément Miège[3], Lincoln H. Pitcher[1], Jonathan C. Ryan[4], Kang Yang[1], Sarah Cooley[1]

[1]Department of Geography, University of California-Los Angeles, CA 90095, USA
[2]Department of Geography, Rutgers, The State University of New Jersey, Piscataway, NJ 08854, USA
[3]Department of Geography, University of Utah, Salt Lake City, Utah, USA
[4]Center for Glaciology, Department of Geography and Earth Sciences, Aberystwyth University, Aberystwyth, United Kingdom

Correspondence to: Matthew G. Cooper (guycooper@ucla.edu)

Abstract. We document the density and hydrologic properties of bare, ablating ice in a mid-elevation (1215 m a.s.l.) supraglacial internally drained catchment near Kangerlussuaq, southwest Greenland. We find water saturated, low-density (474–725 kg m^{-3}, μ=688 kg m^{-3}) ice to at least 1.1 m depth below the ice sheet surface. This near surface, low-density ice consists of alternating fractured porous ice and clear solid ice lenses, overlain by a thin (<0.5 m), even lower density (326-555 kg m^{-3}, μ=455 kg m^{-3}) unsaturated weathering crust. Ice-density data from 10 shallow (0.9–1.1 m) ice cores along an 800 m transect suggest an average 15–22 cm of liquid meltwater storage within this low-density ice. Water saturation of this ice is confirmed through measurable water levels (1–29 cm, μ=10 cm) in 84% of cryoconite holes and rapid infilling of 83% of 1m drilled holes sampled along the transect. Though preliminary, these findings are consistent with descriptions of shallow, depth-limited aquifers in weathering crusts of temperate and polythermal glaciers worldwide, and confirm the potential for substantial transient meltwater storage within porous low-density ice on the Greenland Ice Sheet ablation zone surface. A conservative estimate for the ~63 km^2 catchment yields 0.010–0.014 km^3 of liquid meltwater storage in near-surface, low-density ice. Further work is required to determine whether these findings are representative of broader areas of the Greenland Ice Sheet ablation zone, and to assess the implications for sub-seasonal surface mass balance calculations, surface lowering observations from airborne and satellite altimetry, and supraglacial runoff processes.

1 Introduction

Each summer a vast and complex network of melt ponds, lakes, streams, and rivers forms on the surface of the Greenland Ice Sheet ablation zone in response to surface melting (Chu, 2014; Smith et al., 2015). Current evidence suggests that most or all of this water is efficiently delivered via supraglacial rivers to terminal moulins and, ultimately, to surrounding oceans (Lindbäck et al., 2015; Rennermalm et al., 2013; Smith et al., 2015), reinforcing concerns about Greenland Ice Sheet meltwater contributions to global sea level rise. This hypothesis is reflected in current-generation regional climate and

surface mass balance models of Greenland which represent ice sheet ablation zone surface runoff as a water balance residual between surface water sources (primarily meltwater) and sinks (primarily evaporative losses), with no physical representation of hydrologic processes taking place on the ablation zone bare ice surface (Smith et al., 2015).

Outside of the Greenland Ice Sheet, however, meltwater storage in a degraded, porous "weathering crust" on the bare ice surface of glaciers delays and dampens meltwater delivery to supraglacial channels via porous subsurface flow (Cook et al., 2016; Fountain and Walder, 1998; Irvine-Fynn et al., 2011; Karlstrom et al., 2014; Munro, 2011; Schuster, 2001), and provides a substrate for internal refreezing of meltwater (Hoffman et al., 2014; Paterson, 1972; Schuster, 2001). Weathering crusts are fractured, disintegrated, or "rotten" ice layers that form on the surface of seasonally temperate glaciers (Brandt and Warren, 1993; Fountain and Walder, 1998; Irvine-Fynn et al., 2011; LaChapelle, 1959; Müller and Keeler, 1969; Nye, 1991). Their formation is controlled by a combination of solar radiative heating in the upper ~2 m of ice (Brandt and Warren, 1993; Liston and Winther, 2005) and heat diffusion between ice grains and intergranular meltwater veins (Lliboutry, 1996; Nye, 1991). During summer when near surface ablation zone ice is warmed to the melting point and solar radiation dominates the surface energy balance, these processes expand intergranular meltwater veins (Müller and Keeler, 1969; Nye, 1991), disaggregate ice crystals (Irvine-Fynn, 2008; Larson, 1977), and create permeable, water saturated ice (Irvine-Fynn, 2008; Larson, 1977; Müller and Keeler, 1969). Subsequent lateral drainage of this meltwater through the permeable weathering crust to supraglacial channels reduces near surface ice density, by removing mass with no detectable change in glacier surface height (Hoffman et al., 2014; Müller and Keeler, 1969). As such, mass change during periods of weathering crust development or removal cannot be resolved solely from ice surface elevation changes (Braithwaite et al., 1998; van den Broeke et al., 2008; Müller and Keeler, 1969).

Weathering crust formation has primarily been studied in Antarctica, where subsurface radiative heating produces subsurface melt in otherwise melt-free environments (Brandt and Warren, 1993; Budd, 1967; Hoffman et al., 2014; Liston et al., 1999; Liston and Winther, 2005). Other work has focused on the biological and carbon-cycle implications of weathering crust as a substrate for microbial-rich cryoconite holes (Cook et al., 2010, 2012; Hodson et al., 2010; Irvine-Fynn and Edwards, 2014). Recently, a small body of research has addressed the hydrologic significance of the weathering crust on Arctic glaciers and ice sheets (Cook et al., 2016; Irvine-Fynn, 2008; Karlstrom et al., 2014), where weathering crust meltwater storage varies diurnally and seasonally (Cook et al., 2016), and controls the timing and variability of meltwater delivery to supraglacial rivers via porous subsurface flow (Karlstrom et al., 2014; Munro, 2011). However, no studies have reported physical properties or documented subsurface meltwater storage for the Greenland Ice Sheet weathering crust. When present in the Greenland Ice Sheet ablation zone, the weathering crust would provide a storage reservoir for meltwater and play an unrecognized role in modulating meltwater delivery to moulins and subglacial hydrologic systems (Karlstrom et al., 2014).

In sum, the weathering crust represents an understudied component of the Greenland Ice Sheet hydrologic system with potential implications for surface mass and energy balance budgets (van den Broeke et al., 2008; Wheler and Flowers, 2011), retrieval of mass changes from surface height change observations (Braithwaite et al., 1998; LaChapelle, 1959; Müller and Keeler, 1969), and controls on the supraglacial hydrograph (Karlstrom et al., 2014; Munro, 2011). Our study presents the first measurements of weathering crust physical properties and documents non-trivial meltwater storage within the low-density, near surface ablating weathering crust in a mid-elevation Greenland Ice Sheet supraglacial catchment. We estimate the liquid meltwater storage potential of the study area weathering crust and discuss implications of the findings for meltwater runoff processes, and surface mass balance (SMB) calculations made from surface height change observations and surface energy balance models. Lastly, we suggest future research directions motivated by our findings of near surface liquid meltwater storage on the Greenland Ice Sheet ablation zone surface.

2 Data and methods

During a 7–14 July 2016 field campaign in the middle ablation zone (67.049° N, 49.022° W, 1215 m a.s.l.), in the Kangerlussuaq region of the Greenland Ice Sheet, we measured near surface weathering crust depth, ice density, effective porosity, presence/absence of sub-surface water saturation, cryoconite hole depth, cryoconite hole water levels, and ice surface topography. These measurements were made along an 800 m transect and are used to characterize near-surface meltwater storage in the bare-ice ablation zone study area weathering crust, within a 63.1 km^2 moulin-terminating supraglacial river catchment (Figure 1).

2.1 Density and stratigraphy of near-surface ice

At ten locations at 80 m posting along the 800 m transect, shallow ice cores 0.9–1.1 m deep were drilled with a 7.25 cm diameter Kovacs Mark III mechanical coring system (www.kovacsicedrillingequipment.com). Ice cores were removed from the drill barrel and analysed adjacent to the drilling sites. Core stratigraphy observations recorded in field notes include the presence of liquid water, ice lenses, and air bubbles. Natural breaks were used to separate the cores into individual segments. Each segment's length and diameter was measured to the nearest 0.1 cm with a caliper and weighed to the nearest 0.1 g on an Acculab digital scale. These measurements were used to determine the ice density of each segment. The natural break segmentation yielded a mean sampling interval of 13 ± 6 cm. Individual segments ranged from 3 to 40 cm in length. Measurement error cannot be quantified with known accuracy as each ice core segment was unique. However, based on field inspection of the ice core geometry we consider 1.3 cm accuracy to be conservative. We therefore assign ±10% measurement uncertainty to the ice core volume and corresponding density. We assume no error in the mass measurement. This uncertainty is incorporated into each calculation involving ice core segment volume and density (explained in more detail in Sect. 2.2 and Sect. 2.4).

At six drilling sites, the upper 14–30 cm of ice lacked sufficient cohesion for intact removal with the coring system. To obtain density measurements for this material, undisturbed samples of ice were removed adjacent to the drilling sites with a Snowmetrics (www.snowmetrics.com) 1000 cm^3 wedge-type steel snow density sampler (Fig. 2). In typical usage, the snow density sampler is inserted horizontally into the sidewall of a snow pit to obtain undisturbed snow samples. For our purposes, ice samples were obtained by inserting the 20 cm sampler vertically downward into the ice. After removal, the mass of each sample was recorded to determine the ice density. To our knowledge, this instrument has not previously been used for ice density studies on weathering crust, but was highly effective at removing the upper 20 cm of ice in the study area with negligible disturbance. These measurements provide bulk density estimates for the upper 20 cm sampling depth. The center of mass of these samples was 6.7 cm below the ice surface due to the sampler geometry (see Fig. 2).

Together, the snow sampler and shallow ice core measurements provide depth-density and stratigraphic profiles to depths ranging from 0.9–1.1 m. To retrieve ice from depths greater than 1.1 m, two additional shallow ice cores were drilled to 1.8 m depth (see location in Fig. 1). In both cases, the risk of freezing prevented drilling deeper than 1.8 m and ice density was not measured. Nevertheless, these cores provided valuable qualitative information that is described in Sect. 3.3.

2.2 Effective porosity of near-surface ice

The porosity of the near surface ice was examined to determine the potential liquid meltwater storage capacity of the study area weathering crust. In theory, the total porosity of a solid material is the ratio of pore space volume to total volume and is calculated from the ratio of measured density to pure material density (e.g. Dingman, 2002):

$$\phi_T = 1 - \frac{\rho_M}{\rho_T}, \quad (1)$$

where ϕ_T [-] is total porosity, ρ_M [kg m^{-3}] is measured density, and ρ_T is solid material density [917 kg m^{-3} for pure ice]. If glacier ice did not contain closed pores such as air bubbles that are unavailable for water storage, Eq. (1) would be a straightforward way to calculate ice porosity. However, closed pores represent an unknown proportion of total glacier ice porosity. The "effective" porosity ϕ_{eff}, then, is the ratio of interconnected pore volume to total ice volume, and is the porosity effectively available for water storage. The ϕ_{eff} can be less, but not greater than total porosity. Restated in terms of Eq. (1), this requires that $\phi_{eff} \leq 1 - \frac{\rho_M}{\rho_T}$. Owing to its empirical nature, ϕ_{eff} cannot be calculated but instead must be measured.

To measure ϕ_{eff} we used the 1.0 L weathering crust ice samples extracted with the snow sampler described above. Samples were immediately weighed to determine ρ_M. Liquid water was then applied to the leveled ice-filled sampler until the water level was coincident with the ice surface (i.e., until the interconnected pore space was filled with water). ϕ_{eff} was computed as the ratio of the water volume required to fill the sample to the 1.0 L ice sample volume. We restricted our measurements

of ϕ_{eff} to ice sampled from dry weathering crust, but it was not possible to control for the effect of residual liquid water content. Visible air bubbles and ice crystals were carefully observed for signs of melt or deformation and none were observed.

To estimate ϕ_{eff} throughout the shallow ice core samples (where ϕ_{eff} was not measured) an "error-in-variables" (EIV) linear model (York, 1968) was computed between these coincident point measurements of ϕ_{eff} and ρ_M obtained with the snow sampler. EIV refers to a general class of methods for fitting a straight line to experimental data when measurement errors are present in both the independent and dependent variables. The method has been widely applied in geophysical research when measurement errors are considered important (Brutsaert and Lopez, 1998; Hirsch and Gilroy, 1984; Mann et al., 1998; York, 1968; York et al., 2004). The important feature is that EIV regression accounts for error in both the independent and dependent variables when determining the slope and intercept of the straight line. The model is identical in form to a standard ordinary least squares regression but contains additional error terms:

$$\hat{\phi}^*_{eff} = \alpha + \beta \cdot (\rho^* + \eta) + \varepsilon, \quad (2)$$

where ϕ^*_{eff} and ρ^* are the "true" but unobserved effective porosity and ice density, $\hat{\phi}^*_{eff}$ is the EIV estimate of effective porosity, η and ε are the measurement errors, and α and β are the intercept and slope, respectively. We ascribe ±10% measurement error for both ρ_M and ϕ_{eff}. The exact solution procedure is described in York et al., (2004). The α and β estimates are then applied to the shallow ice core ρ_M to estimate ϕ_{eff} for each shallow ice core segment.

2.3 Depth to liquid water saturation

At 100 locations at 8 m posting along the 800 m transect, the unsaturated weathering crust depth, presence/absence of liquid water saturation within the weathering crust, and height of water within cryoconite holes were measured. The unsaturated weathering crust depth was measured by forcing a Snowmetrics steel pointed depth probe downward until impenetrable ice was encountered. Initial expectations were that these measurements would determine the depth of rotten unsaturated ice, as per Fig. (1) in Müller and Keeler (1969). To check the accuracy of these depth probe measurements, we used a flat bladed shovel to excavate the weathering crust adjacent to several depth probe measurement sites and found the depth probe underestimated the depth relative to the shovel by a few centimetres (not systematically measured). Nevertheless, this depth is used solely as a qualitative description of the weathering crust in Sect. 3.3 and is not meant to be an exact measurement of the unsaturated depth. We discuss this transition between unsaturated and saturated ice in more detail in Sect. 3.3. Second, the presence/absence of liquid water saturation was assessed by drilling a 1 m deep hole into the weathering crust with a standard 5 cm diameter Kovacs drill bit. The drilled holes were monitored for liquid water infilling within 30 minutes as an indication of subsurface water saturation. Third, the height of water in the nearest cryoconite hole was determined by measuring the total depth of each hole and the depth to water in each hole below the surface. The depth to water in the holes

is used as an estimate of the depth to liquid water saturation. Absence of cryoconite holes was noted if none were present within a ~1m radius of the 8 m posting.

2.4 Estimating water storage in the weathering crust

The total volumetric water storage S in the weathering crust is defined as:

$$S = S_P + S_I + S_{CH} + S_{cap}, \quad (3)$$

where S_P is free-draining liquid water storage within the weathering crust ice matrix, S_I is refrozen meltwater within the weathering crust, S_{CH} is liquid water storage in cryoconite holes, and S_{cap} is irreducible liquid water held under capillary tension within the weathering crust. The focus of this paper is S_P, which we estimate with the following relationship:

$$S_P = \phi_{eff} * V_P, \quad (4)$$

where V_P is the volume of saturated porous ice within the weathering crust and ϕ_{eff} is the effective porosity of the saturated porous ice within the weathering crust. Eq. (4) is applied to each segment of porous ice in the excavated ice cores. For each segment, V_P is calculated by multiplying the measured thickness of each segment (after subtracting the thickness of solid impermeable ice lenses and the depth of unsaturated ice) by the ice core segment diameter, and ϕ_{eff} is calculated from each segment's ρ_M (Eq. 2). The ±10% measurement uncertainty estimates for V_P and ϕ_{eff} are combined to yield ±20% uncertainty estimates for S_P. These segment S_P values are then summed across each core and normalized by the cross-sectional area of each core and reported as depths of water. The distinction between solid impermeable ice lenses and porous ice is discussed in Sect. 3.1.

Finally, for illustrative purposes we estimate the potential liquid meltwater storage capacity of the study catchment weathering crust by multiplying the mean upper and lower S_P estimated from the shallow ice cores by the bare ice surface area of the study catchment (63.1 km^2). This calculation is inherently conservative in that it assumes there is zero S_P below the ~1 m depth measured with our field equipment, and excludes refrozen meltwater storage (S_I), storage within cryoconite holes (S_{CH}), and unsaturated storage (S_{cap}) altogether. However, it also assumes the ice density, porosity, and saturation conditions measured along the transect are representative of conditions across the entire catchment. Recognizing this uncertainty, we discuss limits to the interpretation in Sect. 4.1 and caution that it is meant for illustrative purposes.

The Cryosphere Discuss., https://doi.org/10.5194/tc-2017-107
Manuscript under review for journal The Cryosphere
Discussion started: 17 July 2017

3 Results

3.1 Density and stratigraphy of near-surface ice

Throughout the study area, the ice sheet surface was characterized by a layer of coarse grained, disintegrated ice, a few tens of centimetres thick (Fig. 2). Bulk ρ_M of the ice in this layer measured to 20 cm depth with the snow sampler was on average 454 ± 53 kg m^{-3}, much lower than typical glacier ice densities of 830–900 kg m^{-3} (Cuffey and Paterson, 2010). These ρ_M, though surprisingly low, are consistent with previous findings of weathering crust ice densities < 500 kg m^{-3}, attributed to weathering crust internal ablation (Müller and Keeler, 1969). Also, consistent with these previous descriptions, the ice in this layer was unsaturated. For example, free draining liquid water was not observed in the extracted ice samples and there was no subsurface water table observed within this upper disintegrated weathering crust layer when removed with the shovel.

At six of the ten shallow ice core drilling sites, this upper layer of disintegrated ice could not be removed intact with the coring equipment and was discarded. Beneath the disintegrated upper layer, sub-surface ρ_M from the shallow ice cores were on average 672 ± 89 kg m^{-3}, and thus greater than those in the upper disintegrated layer, but consistently lower than solid ice density (Figure 3). Density did not increase consistently with depth, nor was solid ice density reached at the ~1m deep base of any of the shallow cores. Relative to ρ_M in the upper 20 cm, the standard deviation of ρ_M was greater across the depth of the shallow ice cores (53 vs. 89 kg m^{-3}). Nevertheless, the variation of ρ_M with depth was relatively small, except for a few large fluctuations toward very low densities < 500 kg m^{-3} (e.g. Core 2, 5, and 8). Alternating weak and resistant layers were qualitatively observed based on the resistance to downward drilling motion. After removal of the cores, these observations were confirmed by the presence of alternating layers of fractured granular ice and clear solid ice lenses in all cores (Figure 3).

Analysis of the extracted cores revealed layers of fractured, coarse-grained (> 1 cm) ice alternating with clear solid ice lenses with no visible grains but many fine bubbles (Figure 4). The location of each solid ice lens in the stratigraphy of the extracted cores was visually identified and recorded using an ordinary graduated meter stick. After weighing and measuring the core segments to determine ρ_M, the clear ice lenses were separated from the fractured ice and their thicknesses measured with the meter stick. The lenses contained visible closed air bubbles trapped in clear solid ice and were unambiguously distinct from the fractured, granular ice between lenses. Densities of these lenses were not studied in the field but through visible inspection are estimated to be in the range of typical glacier ice densities (830–900 kg m^{-3}; Cuffey and Paterson, 2010), likely on the lower end due to observed trapped air bubbles.

The nature of the solid ice lenses, and a mechanism to explain the observed pattern of alternating clear, solid ice and fractured, granular ice, is difficult to determine. Previous analyses of weathering crusts have not reported this pattern (e.g. Hoffman et al., 2014; Müller and Keeler, 1969; Schuster, 2001). This finding was not anticipated and a detailed investigation

is beyond the scope of this paper. Regardless of mechanism, the presence of these solid ice lenses has two implications for this analysis. First, the ρ_M reported in Fig. 3 were calculated from the mass of each ice core segment measured prior to removing the ice lenses, as it was impossible to remove the lenses without destroying the core segments. The reported ρ_M therefore represent the bulk density of each segment (i.e. weathered ice + solid ice) and are thus biased slightly high relative to the density of the weathered ice in each segment. This is relevant because ρ_M is used to predict ϕ_{eff} for the weathered ice. Though impossible to quantify without knowing the density of each ice lens, this conservative bias propagates directly into conservative estimates of ϕ_{eff} and S_P, and hence is not considered problematic as it decreases the likelihood of overestimating S_P. Second, the ice lenses are assumed to be impermeable based on the visual analysis described above. As noted in Sect. 2.4, the thickness of each lens is subtracted from the thickness of each ice core segment when calculating V_P (Eq. 4).

3.2 Measured and estimated effective porosity

Effective porosity ϕ_{eff} measured with the snow sampler is 0.43 ± 0.05. Measured values were consistently smaller than the theoretical upper bound total porosity (ϕ_T) calculated from ρ_M (Fig. 5). We attribute this to observed closed air bubbles in the porous ice grains that decrease the density without increasing the porosity (and are unavailable to liquid water storage). This result suggests our measurement technique was accurate, as data points above the dashed line in Fig. 5 would be unphysical, and also provides confidence in the empirical regression derived from these measurements (Fig. 5).

A strong linear relationship was found ($\phi_{eff} = -0.97\rho_M + 0.89$; r^2 = 0.53, RMSE = 2.7%). The relationship is robust in physical terms. ϕ_{eff} decreases as ρ_M increases and substituting ρ_M = 0.917 kg m^{-3} into the regression yields ϕ_{eff} = 0. Nevertheless, the narrow range of ρ_M is a source of uncertainty when extrapolating outside of the measurement range (i.e. ϕ_{eff} < 0.35 and ϕ_{eff} > 0.55 have greater uncertainty).

The empirical regression was used to predict ϕ_{eff} from the shallow ice core ρ_M (Figure 3, top axis). Predicted ϕ_{eff} averaged across all core segments is 0.23 ± 0.09 and ranges from 0.0–0.47. Though lower on average than the range of ϕ_{eff} measured with the snow sampler in the upper unsaturated crust, this range suggests substantial porosity across the ~1 m depth sampled with the shallow ice corer. Further, these estimates are likely biased somewhat low due to the effect of including the solid ice lens mass in the ρ_M calculations.

3.3 Evidence of saturation from drilled holes and cryoconite holes

In 83 of 100 drilled 1 m holes, water from surrounding ice infilled the hole within the nominal 30 minute post-drilling observation period. Infilling rates were not systematically measured but were observed to vary from nearly instantaneous

infilling before the drill was removed, to relatively slow infilling over the 30 minute observation period, suggesting substantial spatial variability over short spatial scales.

At each drill site, the depth and water level of the nearest cryoconite hole within a nominal 1 m radius was measured. At 14 sites, no cryoconite holes were present within this 1 m radius. At 8 sites, the nearest cryoconite holes were dry. The remaining 79 of 86 cryoconite holes contained measurable water levels. Cryoconite holes were 25.2 ± 11.4 cm deep and water levels were 9.7 ± 7.8 cm above hole bottoms (vertical blue bars, Fig. 6b).

In addition to the rapid infilling of the majority of drilled 1 m holes and the widespread presence of water filled cryoconite holes, each of the ten shallow ice core boreholes filled with water during the post-drilling period. Collectively, these measurements suggest the ice was saturated across the entire 800 m transect to a depth of at least 1 m, albeit with substantial spatial variability in infilling rates and cryoconite hole water levels.

The ice surface topography along the study transect was highly variable across short spatial scales (<10 m) (Fig. 6). Qualitatively, the surface was characterized by hummocks and hollows separated by shallow rills (often flowing) and pitted cryoconite deposits. Water levels in cryoconite holes generally mirrored the small-scale surface variability and followed the large scale topographic gradient (Fig. 6), suggesting a topographically-driven subsurface water table (e.g. Karlstrom et al., 2014).

Based on these topographic and subsurface water level measurements, depth probe measurements, and shallow ice core stratigraphy, we characterize the near surface ice as consisting of two transient bulk layers. The upper layer consisted of very low-density (< 500 kg m^{-3}), disintegrated, unsaturated weathering crust ice that was readily probed, easily removed with a shovel, and often deformed or collapsed under foot. This upper layer was 11.3 ± 5.8 cm thick as measured with the depth probe (grey shaded area, Fig. 6), with a maximum thickness of 49 cm. Beneath this layer was a saturated, higher density ice layer that we could not excavate with the shovel nor penetrate with the depth probe. Liquid water was often visible just below the transition between layers, made visible when the upper layer was removed with the shovel. Where cryoconite holes were present, their bottoms always extended downward into the lower saturated layer, and the height of water in these holes very rarely extended upward into the unsaturated layer. The cryoconite hole water levels were on average 15.5 cm below the ice sheet surface, and on average 4.2 cm below the estimated bottom of the unsaturated layer as measured with the depth probe (Fig. 6).

The thickness of the lower, saturated ice layer could not be definitively determined with the drilling equipment. However, at two locations shallow ice cores 1.8 m deep were excavated. The density of these cores was not measured, but at both sites the ice cores consisted of fractured, granular ice alternating with clear, solid ice lenses across their entire depth. There were

no qualitative differences between the ice in these cores and the ice presented in Figure 3. At one of these two sites, the pattern of fractured, granular ice persisted to 1.8 m depth. At the other site, a 20-cm thick piece of solid ice was found between 1.6 and 1.8 m, possibly marking the transition to cold, solid ice. At both sites, the drill became difficult to operate and the risk of freezing prevented drilling below 1.8 m. These observations suggest the transition to cold, solid ice at these locations was at or near 1.6–1.8 m deep, and thus provide a plausible estimate for the permeable ice layer depth.

3.4 Estimating meltwater storage in the near-surface ice

While the methods used in this study did not yield a definitive bound on the depth of the saturated ice layer, nor the variation in porosity with depth outside the range of the shallow boreholes, the shallow ice core data allow us to provide plausible bounds for S_P with assumed ±20% measurement uncertainty (Table 1). These estimates are inherently conservative owing to the effect of including the ice lens mass in the density calculation, and they do not include the potential for additional liquid meltwater storage below the measured ice core depths. Averaged across the mean 94 cm depth of the 10 shallow ice cores, S_P is 15–22 cm. The mean depth of porous ice is 73 cm and the mean depth of solid ice lenses is 21 cm.

4 Discussion

Water storage in the weathering crust has been acknowledged but largely dismissed as a significant component of total water storage in polythermal ice sheets, owing to its transient nature (Fountain and Walder, 1998; Müller and Keeler, 1969). While more work is needed to determine the spatial extent and seasonal evolution of the conditions found in this investigation, our documentation of a saturated weathering crust harboring up to 22 cm of liquid meltwater storage supports the possibility of substantial transient water storage on the Greenland Ice Sheet ablation zone surface. Moreover, these results are consistent with observations of substantial water storage within the near surface ice of temperate and polythermal glaciers worldwide. For example, a specific storage rate of 5 mm d^{-1} was found for a supraglacial catchment in Arctic Svalbard (Irvine-Fynn, 2008) and 7 mm d^{-1} in the stagnate Burroughs Glacier, Alaska (Larson, 1977). Given these storage rates, a melt season length of 21–44 days would be required to accommodate the 15–22 cm of liquid meltwater storage found in this study.

The two layer system presented in Fig. 6 is consistent with conceptual models of the near surface weathering crust-cryoconite hole hydrologic system proposed by Irvine-Fynn and Edwards (2014) and Müller and Keeler (1969), and confirms this system is present in the Greenland Ice Sheet ablation zone. The ubiquity of water-filled cryoconite holes, the rapid infilling of drilled holes with liquid water, and the excavation of saturated ice cores to depths of 1.8 m suggests the study area weathering crust acts as a depth-limited aquifer (Irvine-Fynn et al., 2011), storing meltwater in the seasonally-temperate near surface ice and delaying the delivery of meltwater to supraglacial streams and rivers via saturated subsurface flow (Fountain and Walder, 1998; Irvine-Fynn et al., 2011; Karlstrom et al., 2014).

Unlike these previous findings, however, we find a pattern of clear, solid ice lenses alternating with porous, granular ice across the depth of all boreholes. These lenses were an unexpected finding and were not studied in the field. Lacking sufficient data to investigate their nature, we hypothesize that these lenses may be remnant solid glacier ice that has undergone little or no weathering. However, there is evidence that internal refreezing of meltwater occurs in weathering crust on the Dry Valley glaciers in Antarctica (Hoffman et al., 2014), which raises the possibility these lenses are internally refrozen meltwater within the weathering crust ice matrix. Assuming a typical glacier ice density range of 830–900 kg m^{-3} (Cuffey and Paterson, 2010), and the mean ϕ_{eff} estimated from the shallow ice core data (0.23), these lenses would constitute an additional 4.0–4.3 cm of meltwater equivalent within the weathering crust in our study area. While we cannot positively interpret the nature of the ice lenses here, future work should determine if internally refrozen meltwater occurs in the GrIS weathering crust, in particular during seasonal transitions from temperate to cold ice conditions in the ablation zone.

4.1 Estimating meltwater storage capacity of the study catchment weathering crust

While extrapolating these preliminary local scale findings to broader areas of the Greenland Ice Sheet is not justified presently, it is illustrative to consider the potential meltwater storage capacity of the weathering crust across our study catchment, if our shallow ice core data were broadly representative of conditions across its 63 km^2 area. For example, multiplying the lower and upper mean S_P (Table 1) by the bare ice surface area of the study catchment yields 0.010–0.014 km^3 of meltwater storage capacity.

To put these numbers in perspective, one hour of peak discharge measured at the Watson River in Kangerlussuaq during the July 2012 record melt event (Nghiem et al., 2012) was equivalent to 0.0115 km^3 (van As et al., 2017). The study catchment occupies a mere ~2% of the total Watson River ablation zone contributing area (2800 km^2; Lindbäck et al., 2015). Thus, while we do not propose the shallow ice core data are representative of ice density or porosity across vast areas of the Greenland Ice Sheet ablation zone (Fountain and Walder, 1998), even relatively small areas of weathering crust have the potential to buffer large volumes of meltwater transport in the Greenland Ice Sheet ablation zone, even when excluding liquid meltwater storage in cryoconite holes, and other sources of surface detention altogether.

4.2 Implications of weathering crust for surface mass balance processes

These findings of low-density, saturated weathering crust in the Greenland Ice Sheet ablation zone have at least four implications for Greenland Ice Sheet surface mass balance (SMB). First, subsurface meltwater generation within the weathering crust does not lower the ice sheet surface (Braithwaite et al., 1998; LaChapelle, 1959; Müller and Keeler, 1969). Subsequent lateral drainage of internal meltwater through the permeable weathering crust to supraglacial channels (Karlstrom et al., 2014) reduces weathering crust density, by removing mass with no detectable change in surface height. As a result, mass change during periods of weathering crust development may be underpredicted or, during periods of weathering crust removal, overpredicted, if determined solely from ice surface elevation changes (Braithwaite et al., 1998;

LaChapelle, 1959; Müller and Keeler, 1969). In turn, where weathering crust is present, ice surface elevation change measurements cannot be confidently used to calibrate SMB models that assume all meltwater is generated at the solid ice surface with no subsurface melt (van den Broeke et al., 2008). In the Kangerlussuaq region of the southwest Greenland Ice Sheet ablation zone, penetration of shortwave radiation into near surface ice is estimated to generate 20–30% of total summertime melt, possibly rendering ablation stake measurements dubious as short-term model validation datasets in this region (van den Broeke et al., 2008).

Second, subsurface melting within the weathering crust may be widespread in the Greenland Ice Sheet ablation zone but has not been systematically evaluated and is not represented in SMB models for the Greenland Ice Sheet. Thus, models that ignore these processes may miscalculate total meltwater production, energy partitioning, and surface lowering, especially on sub-seasonal timescales (van den Broeke et al., 2008; Hoffman et al., 2014; Paterson, 1972; Wheler and Flowers, 2011). Studies that rely on SMB model output to estimate meltwater production or runoff on the Greenland Ice Sheet ablation zone surface may be affected by these errors. For example, investigations of sub-seasonal coupling between surface melt and dynamic ice motion on the Greenland Ice Sheet typically credit surface meltwater instantaneously to the englacial hydrologic system (Das et al., 2008; Hoffman et al., 2011; Joughin et al., 2008; Schoof, 2010; Zwally et al., 2002). Further, the development and removal of the weathering crust is strongly coupled to sub-seasonal synoptic meteorology. For example, the weathering crust can rapidly ablate away when the surface energy balance is dominated by latent or longwave heat fluxes (Müller and Keeler, 1969; Schuster, 2001). Such conditions are common during warm rainfall events, which have been linked to short term ice-flow acceleration (Doyle et al., 2015). Understanding sub-seasonal ablation processes such as weathering crust development and removal could thus improve our understanding of meltwater delivery to the englacial system.

Third, the weathering crust provides a substrate for cryoconite, the biologically active sediment that darkens the Greenland Ice Sheet ablation zone surface (Benning et al., 2014; Lutz et al., 2014). Cryoconite deposits locally enhance melt, forming narrow cylindrical melt holes that deepen into the weathering crust (Fountain et al., 2004), accumulating cryoconite at their base. This deepening locally brightens the ice surface relative to dispersed or uniform debris covered ice (Boggild et al., 2010). Subsurface water exchange may further redistribute impurities between the permeable weathering crust and cryoconite holes (Cook et al., 2016), while channel invasion of cryoconite holes during periods of weathering crust removal may disperse cryoconite sediments across the ice surface (Hodson et al., 2007; Takeuchi et al., 2000). Thus, while it has not been studied, weathering crust growth and removal could modulate seasonal effects of impurities on albedo patterns in the Greenland Ice Sheet ablation zone.

Finally, typical flow velocities of 0.4–2.6 m s^{-1} in meltwater channels on the Greenland Ice Sheet (Gleason et al., 2016) are 3–5 orders of magnitude greater than hydraulic conductivity estimates for permeable ice (Cook et al., 2016; Fountain and

Walder, 1998; Karlstrom et al., 2014; Wakahama et al., 1973). Thus, subsurface meltwater flow may be the limiting mechanism controlling variability of surface meltwater delivery to supraglacial channels, which in turn deliver meltwater to englacial and subglacial systems. Yet, little is known about the Greenland Ice Sheet weathering crust hydraulic properties that control this flow, in particular the weathering crust hydraulic conductivity. Prior investigations of Greenland Ice Sheet surface hydrologic routing relied exclusively on assumptions of instantaneous meltwater runoff, or routing schemes appropriate strictly for channelized or overland flow (e.g. Arnold et al., 1998, 2014, Banwell et al., 2012, 2013). Hence, understanding subsurface meltwater transport mechanisms in addition to surface transport mechanisms in the Greenland Ice Sheet ablation zone should improve modelling capabilities.

5 Conclusion

The evidence presented in this study suggests a saturated weathering crust is present in summer on the bare ice surface of the Greenland Ice Sheet ablation zone. The observed characteristics of this weathering crust are similar to those described for temperate and polythermal ice masses worldwide (Cook et al., 2016; Hoffman et al., 2014; Irvine-Fynn and Edwards, 2014; Karlstrom et al., 2014; Larson, 1978; Müller and Keeler, 1969; Munro, 2011). Namely, the weathering crust acts as a depth limited aquifer (Irvine-Fynn et al., 2011), storing liquid meltwater and likely slowing its transport to supraglacial streams via porous subsurface flow (Cook et al., 2016; Karlstrom et al., 2014). Our empirical relationship ($\phi_{eff} = -0.97\rho_M + 0.89$) between measured ice density (ρ_M) and measured ice porosity (ϕ_{eff}) at the study field site suggests 15–22 cm of meltwater storage within weathering crust at our study site. Though preliminary, these findings suggest the potential for non-trivial sub-seasonal meltwater storage within porous low density ice on the Greenland Ice Sheet ablation zone bare ice surface. We do not propose that these findings represent typical conditions in the Greenland Ice Sheet ablation zone. More work is needed to determine if the near-surface ice physical properties found at this particular field site are representative of other areas of the ablation zone, and how the weathering crust evolves in response to seasonal changes in the surface energy balance. Future work should examine potential errors in sub-seasonal SMB and surface elevation change estimates derived from surface energy balance models and altimetry, as most currently neglect removal of mass via subsurface melting in the weathering crust.

Data availability

All data is available upon request from the corresponding author and is currently in preparation for submission to an online open access data repository.

Author contribution

M.G. Cooper, L.C. Smith, and A.K. Rennermalm designed the experiment. M.G. Cooper, L.C. Smith, A.K. Rennermalm, C. Miège, L. H. Pitcher, J. Ryan, and S. Cooley collected the field data. J. Ryan assisted with UAS image processing. M.G. Cooper performed the data analysis. M.G. Cooper wrote the manuscript with contributions from all authors. The authors declare they have no conflict of interest.

Acknowledgements

This project was funded by the NASA Cryosphere Program grant NNX14AH93G (P.I. Laurence C. Smith) managed by Dr. Thomas P. Wagner. We thank Professor Robert Hawley of Dartmouth University for the generous lending of the shallow ice core drill. We thank Polar Field Services for their field support, Charlie Kershner (George Mason University), Brandon Overstreet (University of Wyoming), Sasha Leidman (Rutgers University), and Rohi Muthyala (Rutgers University) for their field work assistance.

References

Arnold, N., Richards, K., Willis, I. and Sharp, M.: Initial results from a distributed, physically based model of glacier hydrology, Hydrol. Process., 12(2), 191–219, doi:10.1002/(SICI)1099-1085(199802)12:2<191::AID-HYP571>3.0.CO;2-C, 1998.

Arnold, N. S., Banwell, A. F. and Willis, I. C.: High-resolution modelling of the seasonal evolution of surface water storage on the Greenland Ice Sheet, The Cryosphere, 8(4), 1149–1160, doi:10.5194/tc-8-1149-2014, 2014.

van As, D., Bech Mikkelsen, A., Holtegaard Nielsen, M., Box, J., Claesson Liljedahl, L., Lindbäck, K., Pitcher, L. and Hasholt, B.: Hypsometric amplification and routing moderation of Greenland ice sheet meltwater release, Cryosphere Discuss, 2017, 1–30, doi:10.5194/tc-2016-285, 2017.

Banwell, A. F., Arnold, N. S., Willis, I. C., Tedesco, M. and Ahlstrøm, A. P.: Modeling supraglacial water routing and lake filling on the Greenland Ice Sheet, J. Geophys. Res. Earth Surf., 117(F4), F04012, doi:10.1029/2012JF002393, 2012.

Banwell, A. F., Willis, I. C. and Arnold, N. S.: Modeling subglacial water routing at Paakitsoq, W Greenland, J. Geophys. Res. Earth Surf., 118(3), 1282–1295, doi:10.1002/jgrf.20093, 2013.

Benning, L. G., Anesio, A. M., Lutz, S. and Tranter, M.: Biological impact on Greenland's albedo, Nat. Geosci., 7(10), 691–691, doi:10.1038/ngeo2260, 2014.

Boggild, C. E., Brandt, R. E., Brown, K. J. and Warren, S. G.: The ablation zone in northeast Greenland: ice types, albedos and impurities., , doi:10.3189/002214310791190776, 2010.

Braithwaite, R. J., Konzelmann, T., Marty, C. and Olesen, O. B.: Errors in daily ablation measurements in northern Greenland, 1993-94, and their implications for glacier climate stuthes, J. Glaciol., 44(148), 583–588, doi:10.3198/1998JoG44-148-583-588, 1998.

Brandt, R. E. and Warren, S. G.: Solar-heating rates and temperature profiles in Antarctic snow and ice, J. Glaciol., 39(131), 99–110, doi:10.3198/1993JoG39-131-99-110, 1993.

van den Broeke, M., Smeets, P., Ettema, J., van der Veen, C., van de Wal, R. and Oerlemans, J.: Partitioning of melt energy and meltwater fluxes in the ablation zone of the west Greenland ice sheet, The Cryosphere, 2(2), 179–189, doi:10.5194/tc-2-179-2008, 2008.

Brutsaert, W. and Lopez, J. P.: Basin-scale geohydrologic drought flow features of riparian aquifers in the Southern Great Plains, Water Resour. Res., 34(2), 233–240, doi:10.1029/97WR03068, 1998.

Budd, W.: Ablation from an Antarctic Ice Surface, Phys. Snow Ice Proc. 雪氷の物理学 論文集, 1(1), 431–446, 1967.

Chu, V. W.: Greenland ice sheet hydrology A review, Prog. Phys. Geogr., 38(1), 19–54, doi:10.1177/0309133313507075, 2014.

Cook, J., Hodson, A., Telling, J., Anesio, A., Irvine-Fynn, T. and Bellas, C.: The mass–area relationship within cryoconite holes and its implications for primary production, Ann. Glaciol., 51(56), 106–110, doi:10.3189/172756411795932038, 2010.

Cook, J. M., Hodson, A. J., Anesio, A. M., Hanna, E., Yallop, M., Stibal, M., Telling, J. and Huybrechts, P.: An improved estimate of microbially mediated carbon fluxes from the Greenland ice sheet, J. Glaciol., 58(212), 1098–1108, doi:10.3189/2012JoG12J001, 2012.

Cook, J. M., Hodson, A. J. and Irvine-Fynn, T. D. L.: Supraglacial weathering crust dynamics inferred from cryoconite hole hydrology, Hydrol. Process., 30(3), 433–446, doi:10.1002/hyp.10602, 2016.

Cuffey, K. M. and Paterson, W. S. B.: The physics of glaciers, Academic Press., 2010.

Das, S. B., Joughin, I., Behn, M. D., Howat, I. M., King, M. A., Lizarralde, D. and Bhatia, M. P.: Fracture Propagation to the Base of the Greenland Ice Sheet During Supraglacial Lake Drainage, Science, 320(5877), 778–781, doi:10.1126/science.1153360, 2008.

Dingman, S. L.: Physical hydrology, Prentice Hall, Upper Saddle River, N.J., 2002.

Doyle, S. H., Hubbard, A., van de Wal, R. S. W., Box, J. E., van As, D., Scharrer, K., Meierbachtol, T. W., Smeets, P. C. J. P., Harper, J. T., Johansson, E., Mottram, R. H., Mikkelsen, A. B., Wilhelms, F., Patton, H., Christoffersen, P. and Hubbard, B.: Amplified melt and flow of the Greenland ice sheet driven by late-summer cyclonic rainfall, Nat. Geosci., 8(8), 647–653, doi:10.1038/ngeo2482, 2015.

Fountain, A. G. and Walder, J. S.: Water flow through temperate glaciers, Rev. Geophys., 36(3), 299–328, doi:10.1029/97RG03579, 1998.

Fountain, A. G., Tranter, M., Nylen, T. H., Lewis, K. J. and Mueller, D. R.: Evolution of cryoconite holes and their contribution to meltwater runoff from glaciers in the McMurdo Dry Valleys, Antarctica, J. Glaciol., 50(168), 35–45, doi:10.3189/172756504781830312, 2004.

Gleason, C. J., Smith, L. C., Chu, V. W., Legleiter, C. J., Pitcher, L. H., Overstreet, B. T., Rennermalm, A. K., Forster, R. R. and Yang, K.: Characterizing supraglacial meltwater channel hydraulics on the Greenland Ice Sheet from in situ observations, Earth Surf. Process. Landf., 41(14), 2111–2122, doi:10.1002/esp.3977, 2016.

Hirsch, R. M. and Gilroy, E. J.: Methods of Fitting a Straight Line to Data: Examples in Water Resources1, JAWRA J. Am. Water Resour. Assoc., 20(5), 705–711, doi:10.1111/j.1752-1688.1984.tb04753.x, 1984.

Hodson, A., Anesio, A. M., Ng, F., Watson, R., Quirk, J., Irvine-Fynn, T., Dye, A., Clark, C., McCloy, P., Kohler, J. and Sattler, B.: A glacier respires: Quantifying the distribution and respiration CO2 flux of cryoconite across an entire Arctic supraglacial ecosystem, J. Geophys. Res. Biogeosciences, 112(G4), G04S36, doi:10.1029/2007JG000452, 2007.

Hodson, A., Bøggild, C., Hanna, E., Huybrechts, P., Langford, H., Cameron, K. and Houldsworth, A.: The cryoconite ecosystem on the Greenland ice sheet, Ann. Glaciol., 51(56), 123–129, doi:10.3189/172756411795931985, 2010.

Hoffman, M. J., Catania, G. A., Neumann, T. A., Andrews, L. C. and Rumrill, J. A.: Links between acceleration, melting, and supraglacial lake drainage of the western Greenland Ice Sheet, J. Geophys. Res. Earth Surf., 116(F4), F04035, doi:10.1029/2010JF001934, 2011.

Hoffman, M. J., Fountain, A. G. and Liston, G. E.: Near-surface internal melting: a substantial mass loss on Antarctic Dry Valley glaciers, J. Glaciol., 60(220), 361–374, doi:10.3189/2014JoG13J095, 2014.

Irvine-Fynn, T.: Modelling runoff from the maritime arctic cryopshere: Water storage and routing at Midtree Lovenbreen, Ph.D., University of Sheffield. [online] Available from: http://ethos.bl.uk/OrderDetails.do?uin=uk.bl.ethos.489371 (Accessed 19 January 2017), 2008.

Irvine-Fynn, T. D. L. and Edwards, A.: A frozen asset: The potential of flow cytometry in constraining the glacial biome, Cytometry A, 85(1), 3–7, doi:10.1002/cyto.a.22411, 2014.

Irvine-Fynn, T. D. L., Hodson, A. J., Moorman, B. J., Vatne, G. and Hubbard, A. L.: Polythermal Glacier Hydrology: A Review, Rev. Geophys., 49(4), RG4002, doi:10.1029/2010RG000350, 2011.

Joughin, I., Das, S. B., King, M. A., Smith, B. E., Howat, I. M. and Moon, T.: Seasonal Speedup Along the Western Flank of the Greenland Ice Sheet, Science, 320(5877), 781–783, doi:10.1126/science.1153288, 2008.

Karlstrom, L., Zok, A. and Manga, M.: Near-surface permeability in a supraglacial drainage basin on the Llewellyn Glacier, Juneau Icefield, British Columbia, The Cryosphere, 8(2), 537–546, doi:10.5194/tc-8-537-2014, 2014.

LaChapelle, E.: Errors in Ablation Measurements from Settlement and Sub-Surface Melting*, J. Glaciol., 3(26), 458–467, doi:10.3198/1959JoG3-26-458-467, 1959.

Larson, G. J.: Internal Drainage of Stagnant Ice: Burroughs Glacier, Southeast Alaska, [online] Available from: http://hdl.handle.net/1811/51678 (Accessed 13 October 2016), 1977.

Larson, G. J.: Meltwater Storage in a Temperate Glacier Burroughs Glacier, Southeast Alaska, [online] Available from: http://hdl.handle.net/1811/48914 (Accessed 15 June 2016), 1978.

Lindbäck, K., Pettersson, R., Hubbard, A. L., Doyle, S. H., van As, D., Mikkelsen, A. B. and Fitzpatrick, A. A.: Subglacial water drainage, storage, and piracy beneath the Greenland Ice Sheet, Geophys. Res. Lett., 2015GL065393, doi:10.1002/2015GL065393, 2015.

Liston, G. E. and Winther, J.-G.: Antarctic Surface and Subsurface Snow and Ice Melt Fluxes, J. Clim., 18(10), 1469–1481, doi:10.1175/JCLI3344.1, 2005.

Liston, G. E., Bruland, O., Elvehøy, H. and Sand, K.: Below-surface ice melt on the coastal Antarctic ice sheet, J. Glaciol., 45(150), 273–285, doi:10.3189/002214399793377130, 1999.

Lliboutry, L.: Temperate ice permeability, stability of water veins and percolation of internal meltwater, J. Glaciol., 42(141), 201–211, 1996.

Lutz, S., Anesio, A. M., Villar, J., E, S. and Benning, L. G.: Variations of algal communities cause darkening of a Greenland glacier, FEMS Microbiol. Ecol., 89(2), 402–414, doi:10.1111/1574-6941.12351, 2014.

Mann, M. E., Bradley, R. S. and Hughes, M. K.: Global-scale temperature patterns and climate forcing over the past six centuries, Nature, 392(6678), 779–787, doi:10.1038/33859, 1998.

Müller, F. and Keeler, M.: Errors in Short-Term Ablation Measurements on Melting Ice Surfaces, J. Glaciol., 8(52), 91–105, doi:10.3198/1969JoG8-52-91-105, 1969.

Munro, S. D.: Delays of supraglacial runoff from differently defined microbasin areas on the Peyto Glacier, Hydrol. Process., 25(19), 2983–2994, doi:10.1002/hyp.8124, 2011.

Nghiem, S. V., Hall, D. K., Mote, T. L., Tedesco, M., Albert, M. R., Keegan, K., Shuman, C. A., DiGirolamo, N. E. and Neumann, G.: The extreme melt across the Greenland ice sheet in 2012, Geophys. Res. Lett., 39(20), L20502, doi:10.1029/2012GL053611, 2012.

Nye, J. F.: The rotting of temperate ice, J. Cryst. Growth, 113(3), 465–476, doi:10.1016/0022-0248(91)90081-F, 1991.

Paterson, W. S. B.: Temperature distribution in the upper layers of the ablation area of Athabasca Glacier, Alberta, Canada, J. Glaciol., 11(61), 31–41, 1972.

Rennermalm, A. K., Smith, L. C., Chu, V. W., Box, J. E., Forster, R. R., Van den Broeke, M. R., Van As, D. and Moustafa, S. E.: Evidence of meltwater retention within the Greenland ice sheet, The Cryosphere, 7(5), 1433–1445, doi:10.5194/tc-7-1433-2013, 2013.

Schoof, C.: Ice-sheet acceleration driven by melt supply variability, Nature, 468(7325), 803–806, doi:10.1038/nature09618, 2010.

Schuster, C.: Weathering crust processes on melting glacier ice (Alberta, Canada), Theses Diss. Compr. [online] Available from: http://scholars.wlu.ca/etd/489, 2001.

Smith, L. C., Chu, V. W., Yang, K., Gleason, C. J., Pitcher, L. H., Rennermalm, A. K., Legleiter, C. J., Behar, A. E., Overstreet, B. T., Moustafa, S. E., Tedesco, M., Forster, R. R., LeWinter, A. L., Finnegan, D. C., Sheng, Y. and Balog, J.: Efficient meltwater drainage through supraglacial streams and rivers on the southwest Greenland ice sheet, Proc. Natl. Acad. Sci., 112(4), 1001–1006, doi:10.1073/pnas.1413024112, 2015.

Takeuchi, N., Kohshima, S., Yoshimura, Y., Seko, K. and Fujita, K.: Characteristics of cryoconite holes on a Himalayan glacier, Yala Glacier Central Nepal, Bull. Glaciol. Res., 17, 51–59, 2000.

Wakahama, G., Kuroiwa, D., Kobayashi, D., Tanuma, K., Endo, Y., Mizuno, Y. and Kobayashi, S.: Observations of permeating water through a glacier body, Low Temp. Sci. A, 31, 217–219, 1973.

Wheler, B. A. and Flowers, G. E.: Glacier subsurface heat-flux characterizations for energy-balance modelling in the Donjek Range, southwest Yukon, Canada, J. Glaciol., 57(201), 121–133, doi:10.3189/002214311795306709, 2011.

Yang, K. and Smith, L. C.: Internally drained catchments dominate supraglacial hydrology of the southwest Greenland Ice Sheet, J. Geophys. Res. Earth Surf., 121(10), 2016JF003927, doi:10.1002/2016JF003927, 2016.

York, D.: Least squares fitting of a straight line with correlated errors, Earth Planet. Sci. Lett., 5, 320–324, doi:10.1016/S0012-821X(68)80059-7, 1968.

York, D., Evensen, N. M., Martínez, M. L. and De Basabe Delgado, J.: Unified equations for the slope, intercept, and standard errors of the best straight line, Am. J. Phys., 72(3), 367–375, doi:10.1119/1.1632486, 2004.

Zwally, H. J., Abdalati, W., Herring, T., Larson, K., Saba, J. and Steffen, K.: Surface Melt-Induced Acceleration of Greenland Ice-Sheet Flow, Science, 297(5579), 218–222, doi:10.1126/science.1072708, 2002.

The Cryosphere Discuss., https://doi.org/10.5194/tc-2017-107
Manuscript under review for journal The Cryosphere
Discussion started: 17 July 2017

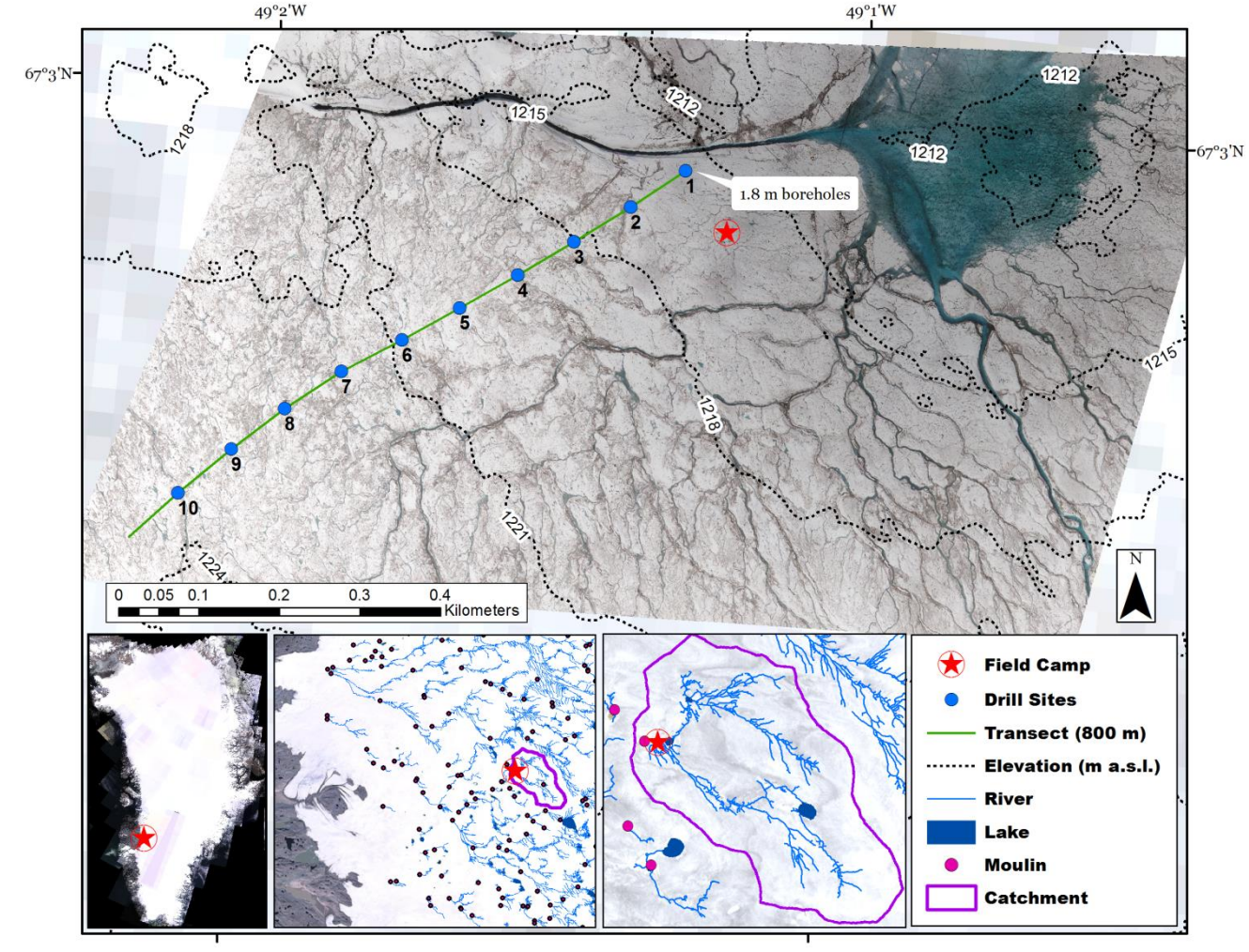

Figure 1: Ortho-rectified image mosaic of the study area at 6 cm ground resolution from RGB camera imagery collected 10 July 2016 on board a quad-copter drone. Background 30 m Landsat image collected same day. Shallow ice cores extracted at 80 m posting (blue circles) along the 800 m transect provide ice density measurements to depths of 1.1 m, with two additional shallow ice cores extracted to 1.8 m depth at posting 1. Insets (below) show the 63.1 km^2 supraglacial catchment extent (magenta outline), as delineated from WorldView satellite stereo-photogrammetric digital elevation model topography, and supraglacial river and moulin locations derived from Landsat 8 imagery (as described in Yang and Smith, 2016).

The Cryosphere Discuss., https://doi.org/10.5194/tc-2017-107
Manuscript under review for journal The Cryosphere
Discussion started: 17 July 2017

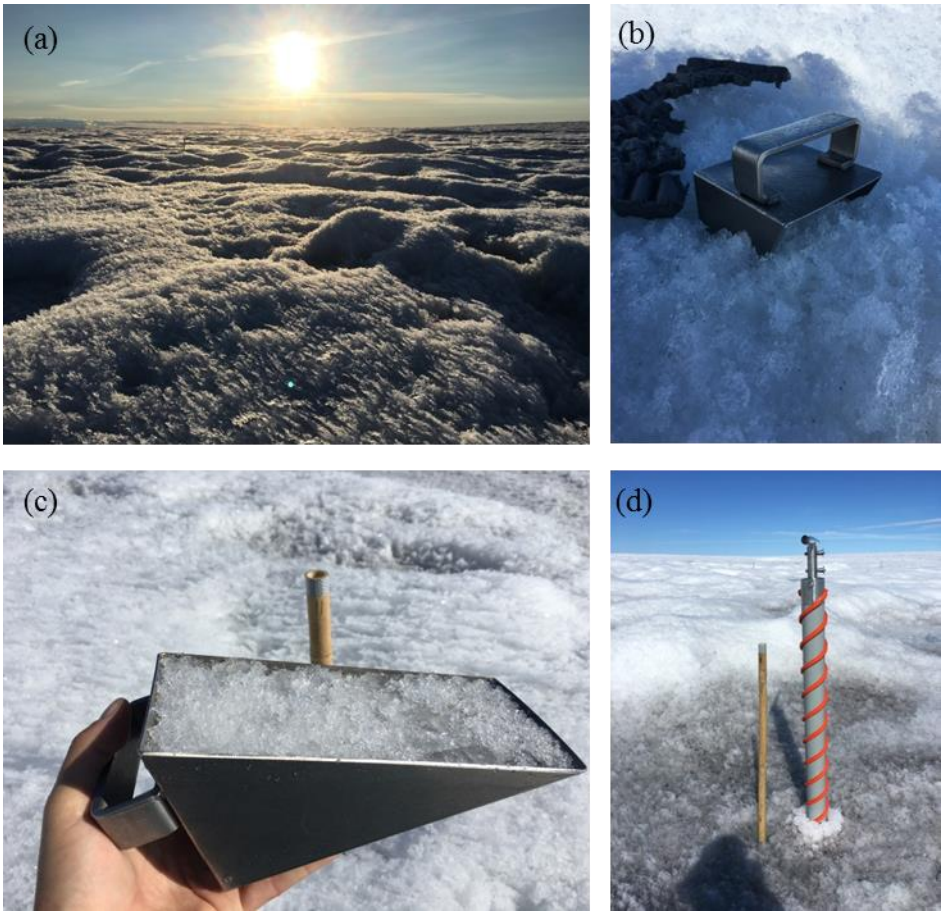

Figure 2: (a) A surface weathering crust was pervasive throughout the study area, characterized by small scale topographic variability and cryoconite holes. (b-c) A 1000 cm^3 steel snow density sampler was vertically inserted into the upper 20 cm weathered ice. (d) A shallow ice core drill was used to obtain ice samples to depths of 1.8 m.

The Cryosphere Discuss., https://doi.org/10.5194/tc-2017-107
Manuscript under review for journal The Cryosphere
Discussion started: 17 July 2017

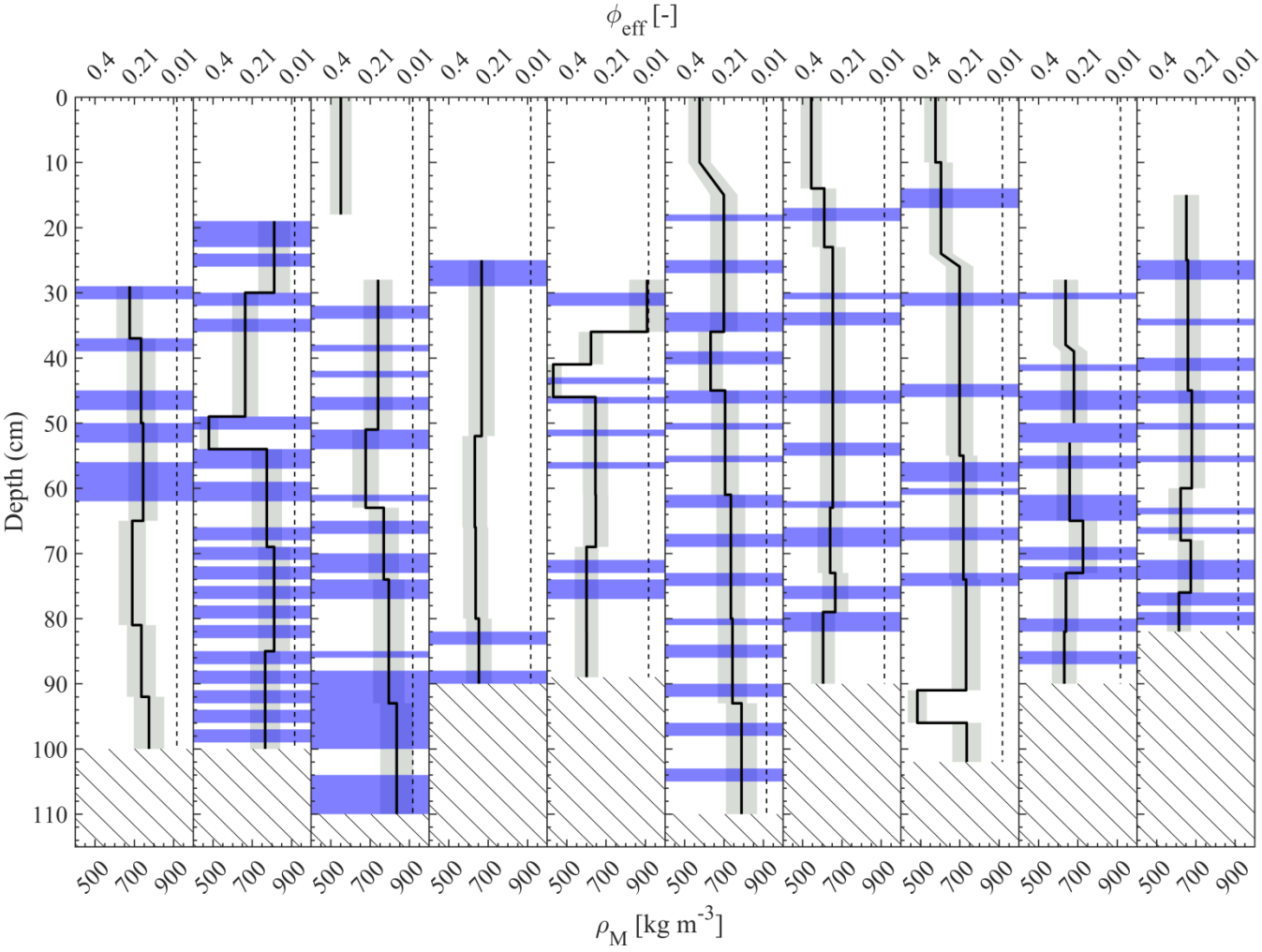

Figure 3: Subsurface measured ice density (ρ_M) and corresponding calculated effective porosity (ϕ_{eff}), and stratigraphy profiles from 10 shallow ice cores (#1-10, left to right) extracted at 80 m postings along the study transect (see Figure 1 for ice core locations). Horizontal blue shading represents solid ice lenses. The ice in between the lenses was granular and porous. Measured ice density (black solid line) was consistently less than solid ice density (917 kg m^{-3}; vertical dashed line). Absence of density data indicates locations where ice lacked sufficient cohesion to measure after removal. Assumed ±10% measurement uncertainty represented by shaded grey bars. Hatched areas represent core depth.

The Cryosphere Discuss., https://doi.org/10.5194/tc-2017-107
Manuscript under review for journal The Cryosphere
Discussion started: 17 July 2017

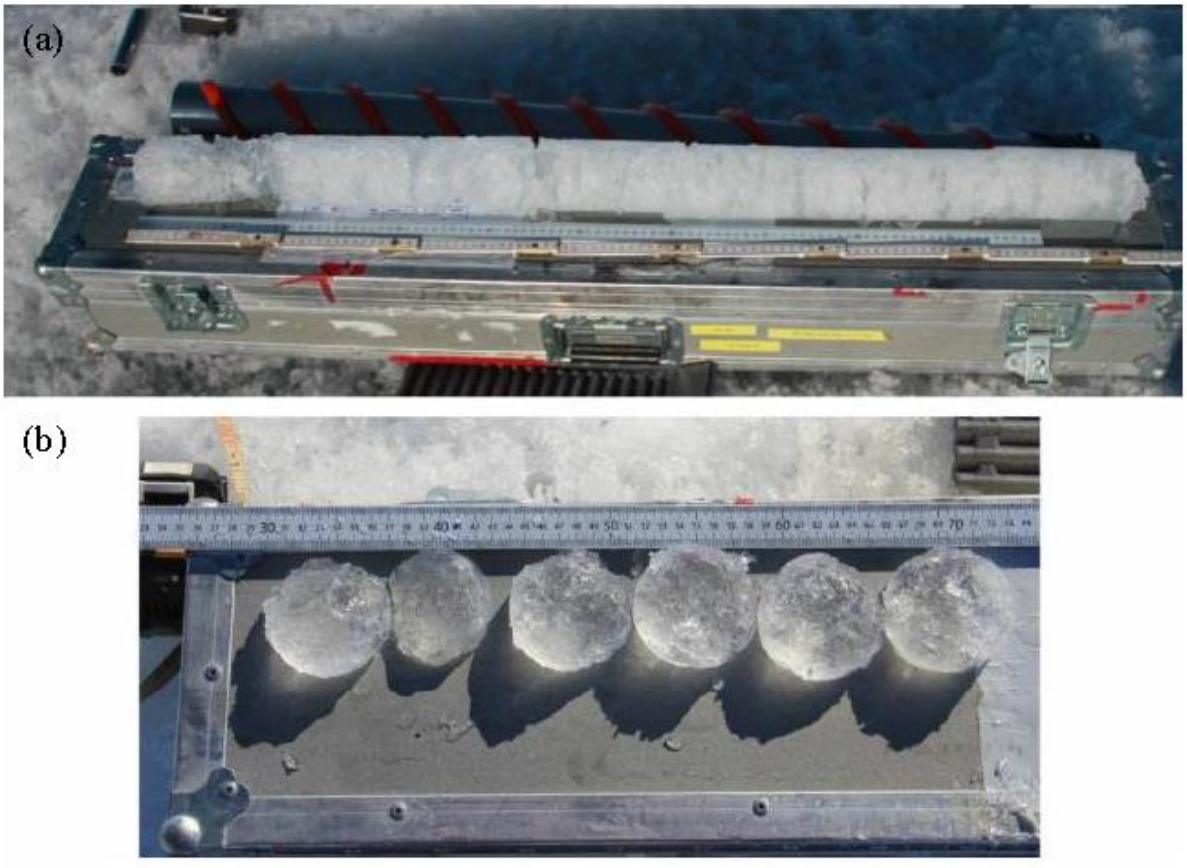

Figure 4: (a) Typical near-surface shallow ice core prior to in situ analysis of density and stratigraphy. Clear, solid ice lenses alternate with granular, fractured ice. (b) Ice lenses removed and confirmed after completed core analysis.

The Cryosphere Discuss., https://doi.org/10.5194/tc-2017-107
Manuscript under review for journal The Cryosphere
Discussion started: 17 July 2017

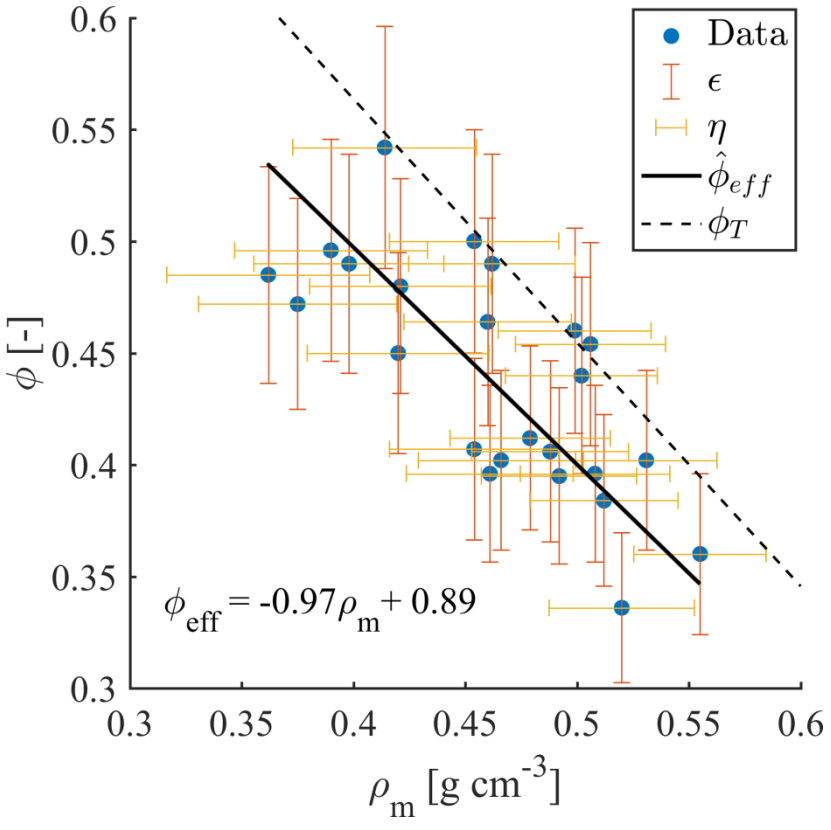

Fig. 5: Linear relationship ($\hat{\phi}_{eff}$, solid line) between measured ice density (ρ_M) and effective porosity (ϕ_{eff}), measured data (blue circles), and assumed ±10% measurement error (whiskers). Dashed line is theoretical upper limit where effective porosity equals total porosity (i.e. $\phi_T = \rho_M/\rho_T$).

The Cryosphere Discuss., https://doi.org/10.5194/tc-2017-107
Manuscript under review for journal The Cryosphere
Discussion started: 17 July 2017

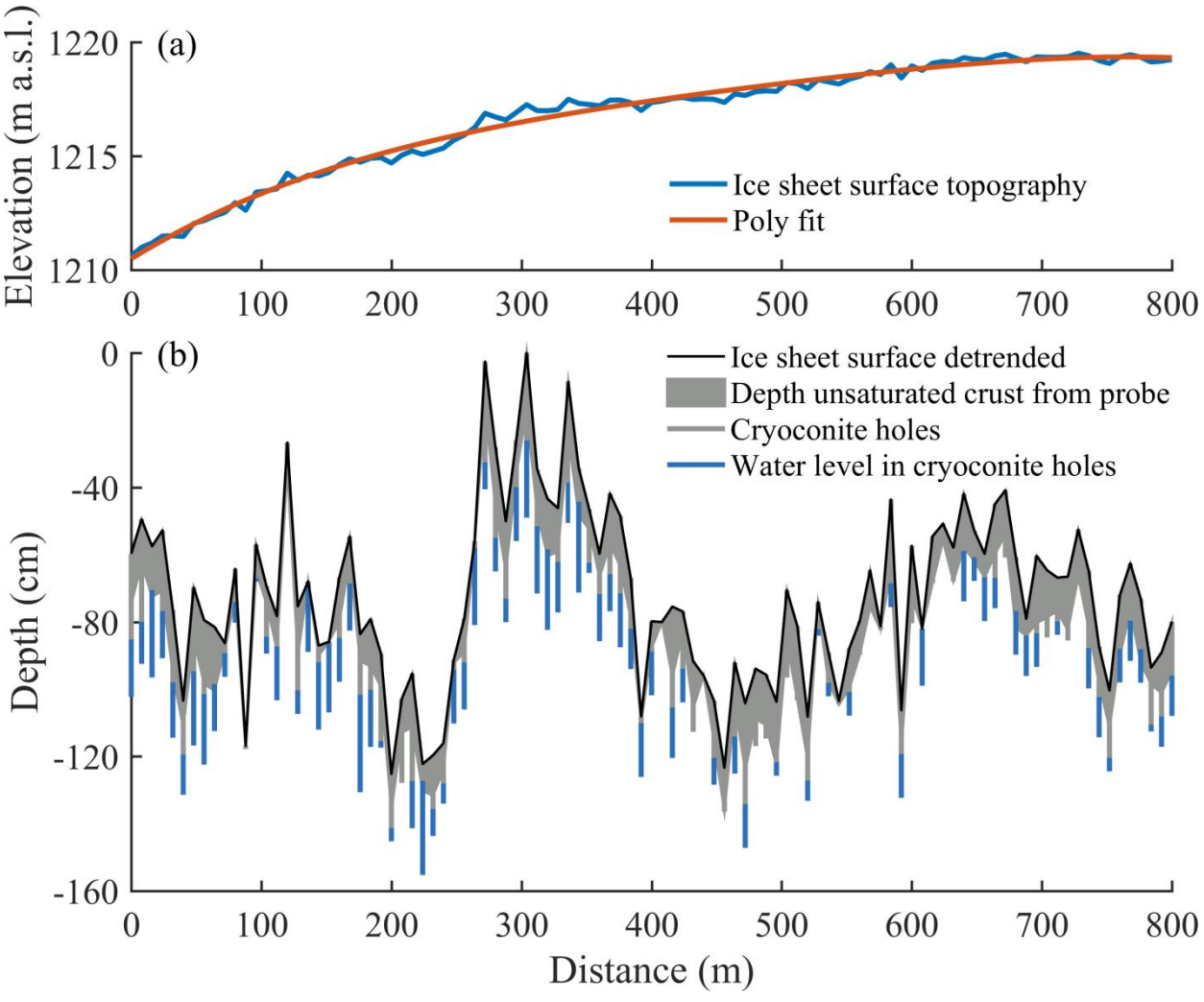

Fig. 6: (a) Ice sheet surface topography along the 800 m study transect extracted from a 6 cm posting stereo-photogrammetric digital elevation model derived from RGB imagery collected 10 July 2016 from a quad-copter drone and the 2nd-order polynomial best fit. (b) Ice sheet surface topography detrended with the polynomial best fit, unsaturated weathering crust depth obtained with the depth probe (shaded grey area), crycoconite hole depths (vertical grey bars), and cryoconite hole water levels (vertical blue bars) sampled along the 800 m study transect

The Cryosphere Discuss., https://doi.org/10.5194/tc-2017-107
Manuscript under review for journal The Cryosphere
Discussion started: 17 July 2017

Table 1: Shallow ice core depth, saturated porous ice depth, solid ice lens depth, and liquid meltwater storage depth (S_P), for each shallow ice core. Upper and lower bounds for S_P are estimated from assumed ±20% measurement error.

Core	Ice Core Depth (cm)	Porous Ice Depth (cm)	Solid Ice Lens Depth (cm)	S_P (cm)
1	100	84	16	11 – 16
2	100	60	40	12 – 18
3	100	63	37	17 – 25
4	90	82	8	14 – 20
`5	89	77	12	15 – 22
6	97	70	27	17 – 25
7	90	72	18	20 – 30
8	102	87	15	19 – 28
9	90	68	22	12 – 18
10	82	63	19	14 – 20
μ	**94**	**73**	**21**	**15 – 22**